SSRG International Journal of Electrical and Electronics Engineering
ISSN: 2348-8379/ https://doi.org/10.14445/23488379/IJEEE-V12I8P106

Volume 12 Issue 8, 46-56, August 2025

Original Article

Integrated Urine Crystal Detection and Classification Using Sensor Data and YOLOv8 Imaging

Joshua V. Nogalo[1], Jovito Miguel R. Regalado[2], Kim P. Ravida[3], Jazel A. Rivera[4], Rosanna C. Ucat[5]

[1,2,3,4,5]*College of Engineering, University of Southeastern Philippines, Davao City, Philippines*.

[3]*Corresponding Author : kpravida@usep.edu.ph*

Received: 04 June 2025 Revised: 06 July 2025 Accepted: 05 August 2025 Published: 30 August 2025

Abstract *- Kidney stones are a prevalent and painful urological condition affecting up to 10% of the global population, particularly men aged 30 to 60. Early detection is essential to prevent complications such as nephrolithiasis and chronic kidney disease. This study presents an integrated system that combines chemical and imaging-based urine analysis to detect and classify urine crystals while measuring pH and turbidity. The system utilizes a pH sensor (PH-4502C) and a turbidity sensor (SENO189), whose outputs are interpreted through logistic regression. Imaging is conducted using a Raspberry Pi High-Quality Camera mounted on a microscope, and crystal classification is performed using the YOLOv8 object detection model trained on labeled datasets of calcium oxalate and triple phosphate crystals. All modules are operated through a Raspberry Pi 4 Model B. Validation with 30 clinical urine samples demonstrated high concordance with standard laboratory results. The system achieved an R^2 value of 0.983 for pH detection, 96.67% accuracy in turbidity classification, and an R^2 of 0.976 with a mean absolute error of 0.733 for crystal counting. Overall risk assessment achieved 96.67% accuracy, 100% precision, 88.89% recall, and an F1 score of 94.12%. These results confirm the system's accuracy, reliability, and suitability for practical use. It offers a low-cost, noninvasive, and real-time solution for early kidney stone detection, with strong potential for application in point-of-care diagnostic settings.*

Keywords *- Kidney stones, Urine crystals, pH sensor, Turbidity analysis, YOLOv8, Raspberry Pi.*

1. Introduction

Renal calculi, often referred to as kidney stones, are a common and painful condition in urology, frequently leading to complications such as nephrolithiasis and urolithiasis [1]. These conditions pose a substantial global health burden, affecting an estimated 12% to 15% of the population [2]. The rising prevalence of kidney stones, which disproportionately impacts men between the ages of 30 and 60, is a growing public health concern [3]. Studies have shown that kidney stones are three times more common in men than women [4], with a male-to-female ratio of approximately 3:1 [5]. Urolithiasis remains one of the most frequent urological diseases globally, accounting for about 40% of urinary disorders [3]. The global incidence of kidney stones continues to rise, especially in developed countries, where cases occur at a rate of eight per 1,000 individuals annually [6]. In Asia, urolithiasis prevalence ranges from 1% to 19.1%, with calcium oxalate as the primary stone component [7, 8]. This increase is largely attributed to lifestyle factors such as high-fat and high-sugar diets [8]. Kidney stones have been linked to higher risks of Chronic Kidney Disease (CKD), cardiovascular issues, and metabolic syndrome [7]. In the Philippines, CKD accounts for 3.5% of deaths, with Davao City ranking third for kidney diseases since 2017 [9].

Given the risks associated with kidney stones, early detection is vital for effective treatment and prevention. While previous studies have employed either urine parameter monitoring or image-based classification using deep learning, these approaches have been explored separately. Sensor-based systems have demonstrated the ability to assess urine quality by measuring pH, turbidity, or ion concentrations, but they lack microscopic analysis capabilities. Conversely, image-based models have successfully detected and classified urine crystals, yet do not incorporate supporting chemical data. This separation limits the diagnostic potential of each method when used independently, especially in detecting early indicators such as crystalluria.

This study addresses this gap by proposing a compact, noninvasive system that integrates sensor-based urine analysis and YOLOv8-powered crystal detection. Combining pH and turbidity measurements with real-time image classification of calcium oxalate and triple phosphate crystals offers a more holistic approach to early kidney stone risk assessment. Unlike earlier efforts that focused solely on either chemical or image data, this work introduces a dual-modality solution that enhances diagnostic precision and supports point-of-care applicability in resource-constrained environments.

2. Related Study

2.1. Kidney Stone Prevalence and Detection Gaps

Kidney stone disease is an increasingly prevalent medical issue affecting patients and healthcare systems [10]. Its prevalence has reached over 10% in countries with reliable health records [5], with notable increases in regions such as Congo, Eswatini, Gabon, and across the Caribbean and Africa [11]. Early detection remains essential due to the high cost and complexity of treating advanced kidney disease and its complications [12]. Despite existing diagnostic practices, the fragmented use of either chemical or imaging-based analysis in isolation limits early detection effectiveness. The study responds to the identified limitation by combining both techniques for a more comprehensive diagnostic profile.

2.2. Traditional Methods and Limitations

Standard diagnostic approaches for kidney stones include reviews of medical history, physical exams, and laboratory tests like blood and urine analysis [13, 14]. Blood tests evaluate factors such as calcium and uric acid levels to assess kidney function [15]. On the other hand, 24-hour urine collection can detect infections, abnormal pH, or elevated mineral concentrations [16]. These tests provide initial insights into metabolic conditions that promote stone formation. Conversely, imaging methods such as X-rays, CT scans, and ultrasound are typically used to visualize stone presence [13, 16]. CT scans are both highly sensitive and specific but carry cost and radiation concerns [14]. Ultrasound, on the other hand, offers a safer and more affordable option but is less reliable for small or obstructed stones [17-19]. Advancements in detection tools have aimed to overcome these pressing limitations. Techniques like gas chromatography-mass spectrometry and Generative Adversarial Networks (GANs) demonstrate potential in metabolic profiling and enhanced image analysis [20]. However, many of these innovations remain in the exploration stage or lack point-of-care adaptability.

2.3. Urine Parameters and Their Diagnostic Value

Among urine indicators, pH and turbidity are closely tied to stone formation. Urinary pH influences the type of stones that form; acidic urine promotes uric acid stones, while alkaline urine favors calcium carbonate stones [21]. Measuring pH and oxalate levels, especially in children, can aid in early screening [22]. However, diurnal variations and sample acidification may affect readings [23]. Turbidity, reflecting the concentration and behavior of solutes, also plays a role. It marks crystal formation phases that include nucleation, growth, and aggregation [24]. Advanced imaging and spectrophotometry techniques now use turbidity and Hounsfield units to estimate crystal types and sizes [25]. Crystalluria, or the presence of crystals in urine, is another key indicator. Calcium oxalate monohydrate crystals are particularly common and are tied to low urine volume, high concentration, and oxidative stress, all of which contribute to stone formation [26]. These crystals damage renal cells and facilitate stone growth [27]. Research into their crystallization process and inhibitors continues to be a major focus [28].

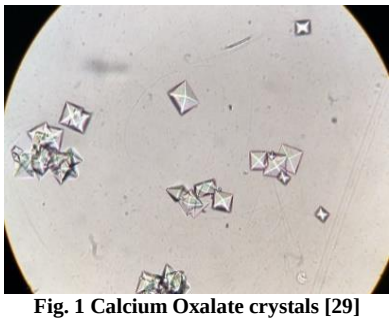

Fig. 1 Calcium Oxalate crystals [29]

Triple phosphate (struvite) crystals, associated with infections by urease-producing bacteria, form in alkaline urine and have distinctive shapes [30]. Their presence typically indicates infection and requires further evaluation.

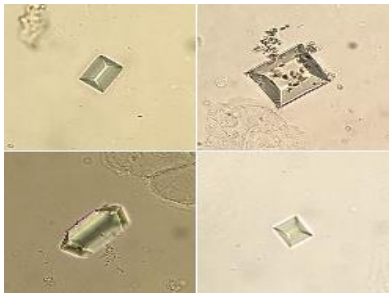

Fig. 2 Triple Phosphate crystals [31]

2.4. Existing Sensor-Based and Imaging-Based Approaches

Recent advances in kidney stone detection have explored both sensor-based and imaging-based systems to improve diagnostic accuracy and clinical utility. On the sensor side, Chung et al. [32] developed a portable system that measured pH, calcium ion concentration, uric acid, and conductivity using a combination of microcontrollers and logistic regression. While this system provided reliable risk assessment, it did not include microscopic imaging, which remains essential in urinalysis, particularly for detecting crystalluria. Similarly, Yudhana et al. [33] designed a system that utilized commercially available sensors to measure pH, turbidity, and ammonia in urine samples. Although this study achieved high accuracy in detecting urine parameters, it was not specifically designed to evaluate kidney stone risks. It did not incorporate any form of visual or image-based analysis. In contrast, image analysis approaches have demonstrated promising results in the classification of urine crystals. Balbin et al. [34] implemented a system using Haar features, Adaptive Boosting, and Support Vector Machine classifiers to detect calcium oxalate and triple phosphate crystals from urine sediment images, reporting over 90% accuracy. Building on this direction, Akhtar et al. [35] introduced an image detection model based on YOLO version 8 to identify visible urine sediment components quickly and accurately. While these image-based methods effectively detect and classify crystals,

they do not incorporate chemical parameters such as pH or turbidity, which are equally essential to contextualize the presence and detected type of crystals. Both sensor and imaging-based systems have shown individual effectiveness, but they function in isolation and fail to provide a holistic approach. There remains a clear need for an integrated system that draws from the strengths of both techniques to enhance early and reliable detection of kidney stone risks.

2.5. Research Gap Analysis

Despite the usefulness of existing systems, there is a distinct limitation in relying on either physical or visual urine analysis alone. Dedicated sensor-based systems are limited in that they cannot confirm the presence, type, or count of urinary crystals, while imaging systems are unable to interpret the chemical environment that promotes crystal formation. Parameters such as pH and turbidity play a critical role in determining the conditions that lead to crystallization [21, 24, 26], yet these are often excluded from image-based diagnostic tools. Developing an integrated system for urine crystal detection and classification that combines sensor data and imaging offers a promising approach to improve diagnostic accuracy in urinalysis, which is vital in monitoring renal and systemic health [36]. YOLO-based deep learning models have demonstrated adequate performance in detecting urine particles like red and white blood cells, epithelial cells, and crystals [36-38].

More so, optimized YOLOv8 versions achieve high precision and mAP scores, effectively dealing with variations in microscopic images [36-38]. However, dedicated imaging systems may struggle in cases of poor image quality or elusive visual cues. Combining sensor data with imaging improves interpretation by providing an added context. Parameters like pH, conductivity, and turbidity can indicate abnormalities prior to visible crystal formation. Hence, the combined setup helps the system identify hidden risks to prompt further analysis when sensor readings raise concerns [39, 40]. Merging YOLOv8's detection capability with sensor input can therefore create a more reliable tool for early detection and reduce false negatives due to human error [36, 40]. The system also follows ensemble principles, using logical operations to enhance decision-making reliability, as demonstrated in related studies [41]. Traditional urinalysis, which depends on manual microscopic assessment, can also vary with technician expertise [42]. Thus, the proposed multi-modal approach in the system attempts to solve the limitations of earlier methods, leading to a more consistent, early identification of kidney stone risks.

3. Materials and Methods

This study employed a structured engineering approach to design and develop an automated urine crystal detection and classification system. The system combines chemical sensor measurements with deep-learning-based image analysis to identify early indicators of kidney stone formation.

3.1. System Block Diagram and Flowchart

The overall system block diagram, as illustrated in Figure 3, presents the combined framework of the urine crystal detection and classification system. It outlines the processes beginning with urine sample acquisition, which is followed by sensor data collection and image capturing.

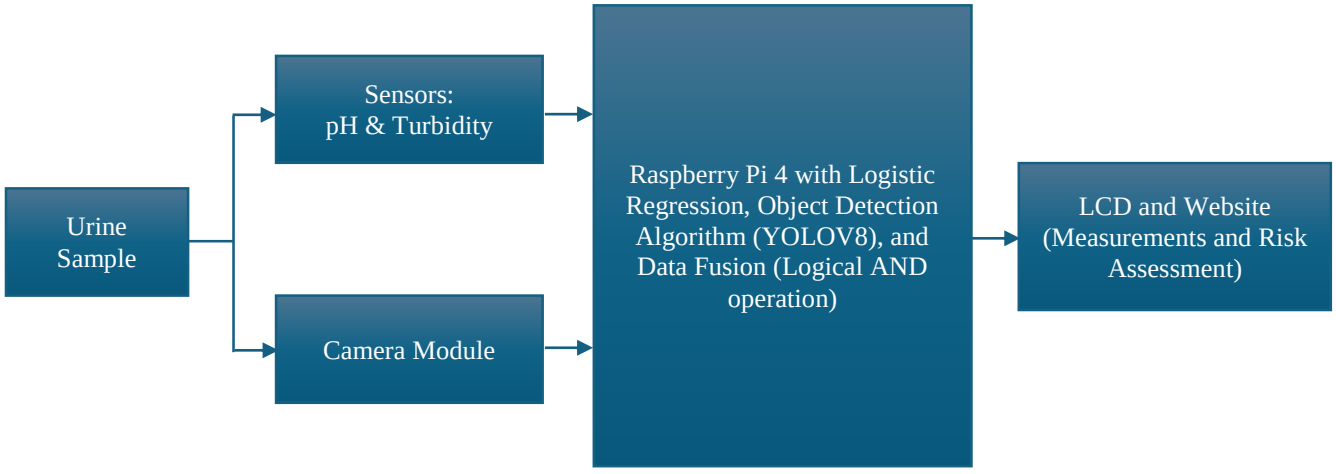

Fig. 3 Overall system block diagram

These inputs are processed in the microcontroller and later subjected to logistic regression. To further illustrate the operational logic of the system, a flowchart is presented that outlines the step-by-step representation of its internal processes. It details how the process takes place from urine sample collection and handling to data acquisition via sensors and imaging. This is followed by analysis through logistic regression and YOLOv8 detection.

Finally, the results from these two streams are then combined using a logical AND operation to arrive at a conclusive kidney stone risk assessment.

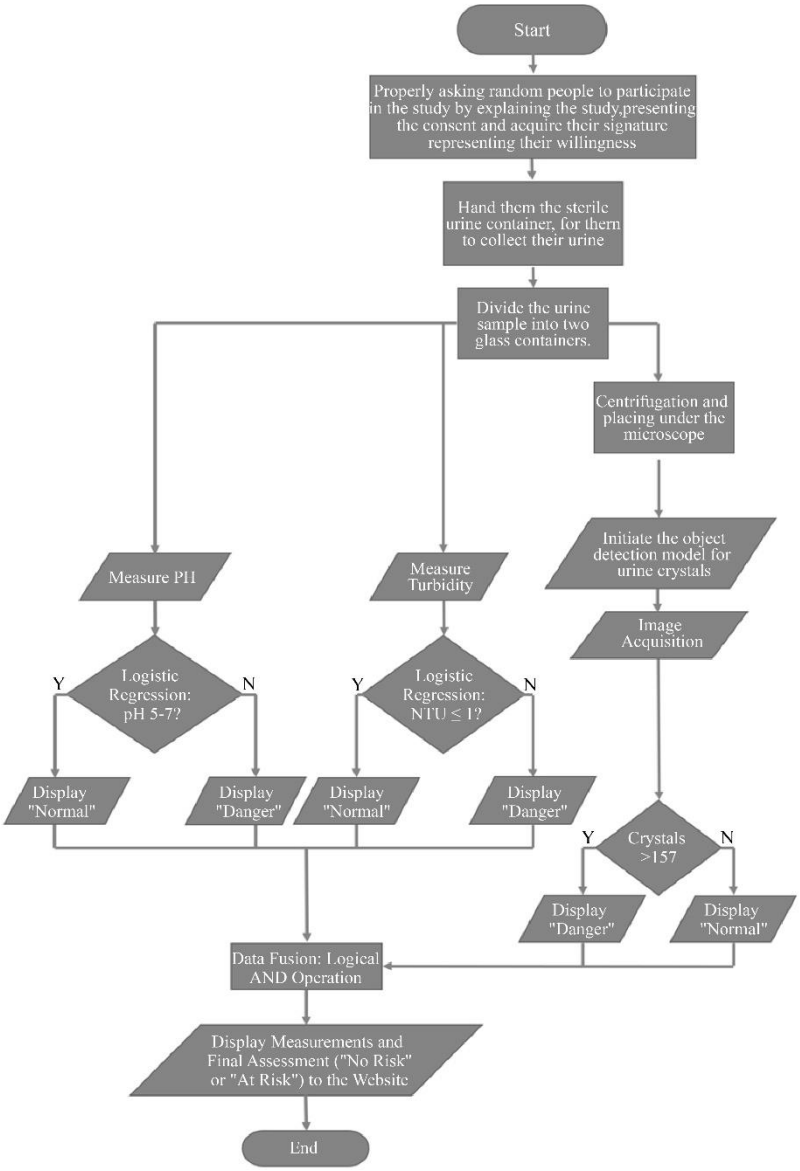

Fig. 4 System flowchart

This flowchart serves as a guide to understand the overall decision process of the system.

3.2. Sample Preparation

The entire process begins with the acquisition of quality samples. For this study, urine samples were collected from volunteer patients at Life Care Medical and Diagnostic Center in Davao City and placed in sterile containers. To ensure reliability, sensor measurements were performed within one hour of collection. Moreover, samples for imaging were centrifuged, and the sediment was transferred to a microscope slide for visual analysis.

3.3. System Architecture

The system architecture is structured into three main functional parts: the input, processing and output modules.

3.3.1. Input Module

The input module is composed of the PH-4502C pH sensor, the SENO189 turbidity sensor, and the Raspberry Pi High-Quality Camera. These components gather both chemical and visual data from the collected urine samples. The chemical analysis is handled by the PH-4502C pH sensor, which was used to measure the acidity or alkalinity of urine.

Fig. 5 PH-4502C pH sensor

This sensor operates within the standard pH scale of 0 to 14, where values below 4.6 are considered highly acidic and those above 8 are considered basic, both conditions being relevant to kidney stone formation.

On the other hand, the SENO189 turbidity sensor was employed to assess urine clarity. This sensor detects the degree of light scattering caused by suspended particles in the liquid, offering insights into the presence of crystals or sediments. Such measurements may indicate early stages of stone development.

Fig. 6 SENO189 turbidity Sensor

The system employed a Raspberry Pi High-Quality Camera with a 12.3-megapixel sensor for image-based analysis. This is connected via the Camera Serial Interface to the Raspberry Pi 4 model B microcontroller.

Fig. 7 Raspberry Pi High-quality camera

The said camera is paired with a microscopic eyepiece adapter. This enables the capture of high-resolution images of urine sediments necessary for crystal detection and classification. All together, these components provided the multi-modal input required for the integrated diagnostic approach.

3.3.2. Processing Module

The inputs gathered are processed in the processing module. Sensor data is interpreted using logistic regression, while the captured images undergo object detection and classification using the YOLOv8 deep learning model.

The processing section was mainly anchored on the Raspberry Pi 4 model B. This compact and high-performance microcontroller served as the central unit for managing data flow and executing the analysis algorithms.

Fig. 8 Raspberry Pi 4 model B

Sensor readings for pH and turbidity were processed using logistic regression. Logistic regression is a statistical method that predicts a binary outcome based on one or more input parameters. In this context, the logistic model interpreted whether the measured values indicated a potential risk associated with kidney stone formation.

The system also analyzed images using You Only Look Once version 8 (YOLOv8), a deep learning model highly regarded for its fast and accurate object detection. YOLOv8 analyzed images captured from urine sediment samples to detect and classify the presence of calcium oxalate and triple phosphate crystals, using bounding boxes to isolate and count crystal types. A logical AND operation was implemented to fuse the preliminary outputs from both the sensor and imaging modules to arrive at a final diagnostic decision. This operation ensured that a positive risk assessment was only concluded when both chemical indicators and crystal presence were aligned, enhancing diagnostic accuracy through multi-layered data validation.

3.3.3. Output Module

Finally, the output module presents the analysis results either on an integrated LCD screen or through a locally hosted web interface, providing accessible and real-time diagnostic feedback to users. All components were controlled via a Raspberry Pi 4 Model B—the Arduino Nano pre-processed sensor signals before sending data to the Raspberry Pi for analysis.

Fig. 9 Implemented pH and turbidity device

Fig. 10 Implemented crystal assessment device

The output of the system integrates with a locally hosted web interface that works alongside the LCD screen to display real-time measurement data and risk assessments. The LCD screen shows the pH and turbidity values immediately, while the web interface provides a centralized platform for data logging and patient record management. Connected to the Raspberry Pi through a local network, the system automatically posts results from both the sensor and imaging modules to the website's homepage.

After entering patient details, the information is stored on the data logging dashboard. The web interface includes a secure login, a results display page, and a dashboard for record tracking, allowing health workers to access and manage patient assessments easily.

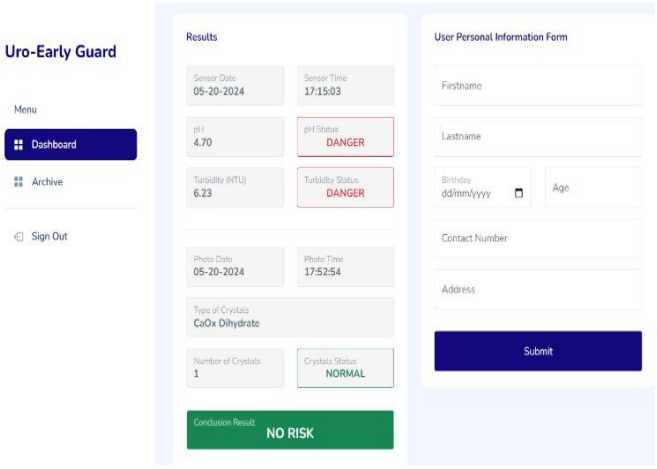

Fig. 11 Website Dashboard

The system architecture demonstrates a well-coordinated integration of sensor measurements, image processing, and data fusion, enabling a comprehensive and reliable approach to early kidney stone risk assessment.

3.4. Sensor Calibration and Data Acquisition

Sensor calibration was performed using buffer solutions and known turbidity samples. Readings were collected, logged, and interpreted using logistic regression to determine abnormal values.

3.5. Image Capture and Model Training

The camera, mounted on a microscope using an eyepiece adapter, captured 12.3 MP images of urine sediments. Image data was annotated and preprocessed using Roboflow. To maintain real-time classification speed, the system did not employ image preprocessing during actual operation; nevertheless, the results were carefully validated against actual clinical findings to ensure reliability and accuracy.

The YOLOv8 model was trained on a dataset of 1,800 labeled images, with a 70:30 training-validation split. The model outputs included crystal counts and type classifications.

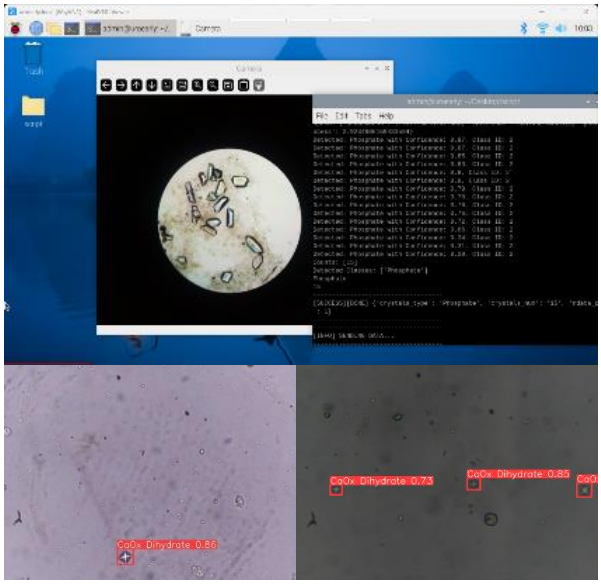

Fig. 12 Testing of the crystal assessment device

The figure shows the actual images captured during the testing phase of the implemented crystal assessment device, illustrating the system's ability to detect and classify urinary crystals in real urine samples.

3.6. System Validation

The system was validated using 30 clinical samples. Sensor readings and YOLOv8 outputs were compared with clinical urinalysis and manual microscopic examination. Performance metrics such as R^2, accuracy, MAE, MSE, and RMSE were used for evaluation.

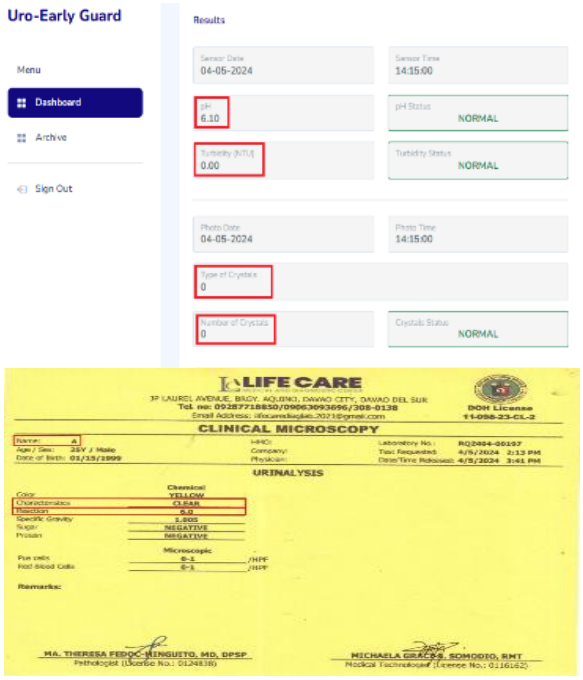

Fig. 13 Comparison of developed system results and clinical results

4. Results and Discussion

This section evaluates the system's performance in terms of pH measurement, turbidity classification, and crystal detection using urine samples. A total of 30 urine samples were examined and compared to clinical standard results.

4.1. pH Measurement Accuracy

The readings of the pH sensor were compared against standard pH strip results. The comparison demonstrated a high correlation, with a coefficient of determination $R^2 = 0.983$.

Table 1. Comparison of pH and turbidity measurements

Sample No.	Clinical Measurement		System Measurement	
	pH	***Turbidity (Clear or Hazy)***	***pH***	***Turbidity (0-1 NTU = Clear, >1 NTU = Hazy)***
1	6.0	Clear	6.1	Clear
2	5.0	Hazy	5.3	Hazy
3	6.5	Hazy	6.7	Hazy
4	6.0	Clear	6.1	Clear
5	6.0	Clear	6.0	Clear
6	6.0	Clear	6.0	Clear
7	6.0	Hazy	6.1	Hazy
8	6.0	Hazy	6.0	Hazy
9	6.0	Hazy	6.0	Hazy
10	5.0	Clear	5.2	Clear
11	7.0	Clear	7.0	Clear
12	6.0	Clear	6.0	Clear
13	6.0	Hazy	6.0	Hazy
14	6.0	Clear	6.2	Clear
15	3.5	Hazy	3.6	Hazy
16	9.0	Hazy	8.7	Hazy
17	4.0	Hazy	3.8	Hazy
18	8.0	Hazy	7.7	Hazy
19	8.0	Hazy	7.9	Hazy
20	9.0	Hazy	8.7	Hazy
21	4.5	Hazy	4.7	Hazy
22	5.0	Hazy	4.9	Hazy
23	5.0	Hazy	4.8	Hazy
24	6.0	Clear	6.0	Clear
25	6.5	Clear	6.2	Clear
26	6.0	Slightly Hazy	6.2	Clear
27	6.0	Clear	6.0	Clear
28	5.0	Clear	5.1	Clear
29	6.0	Hazy	6.3	Hazy
30	5.0	Clear	5.2	Clear

The results indicate a strong agreement between the two measurement methods, closely following the pattern of the clinical reference measurements. The coefficient of determination is calculated using the formula:

$$R^2 = 1 - \frac{RSS}{TSS} \quad (1)$$

RSS is the residual sum of squares, showing the total squared differences between predicted and actual values, while TSS is the total sum of squares. This validates the reliability of the PH-4502C sensor within the system.

4.2. Turbidity Classification Performance

Turbidity was assessed using the SENO189 sensor and classified as either "Clear" or "Hazy" based on a threshold of 1 NTU. Compared to clinical and visual assessments, the system achieved an overall accuracy of 96.67%, confirming its suitability for detecting suspended particulates related to crystalluria. The accuracy was computed using the formula:

$$Accuracy = \frac{No.of\ correctly\ classified\ samples}{Total\ number\ of\ samples} \quad (2)$$

This high accuracy indicates that the sensor's classification capability aligns well with clinical evaluations.

4.3. Crystal Counting Evaluation

The system's ability to count crystals was also assessed. Images of urine sediment were captured using the Raspberry Pi High-Quality Camera and analyzed using the YOLOv8 model. The system's crystal counts were compared with those obtained through manual counting by laboratory professionals.

Table 2. Comparison of crystal counts

Sample No.	Clinical Measurement		System Measurement	
	Clinical Analysis (Descriptions: Normal = Rare or Moderate, Abnormal = Many)		***Clinical Analysis (Descriptions: Normal = Less than or equal to 15 crystals Abnormal = Greater than 15)***	
	No. of Crystals	***Description***	***No. of Crystals***	***Description***
1	0	-	0	-
2	0	-	0	-
3	0	-	0	-
4	0	-	0	-
5	0	-	0	-
6	0	-	0	-
7	0	-	0	-
8	0	-	0	-
9	0	-	0	-
10	0	-	0	-
11	0	-	0	-
12	0	-	0	-
13	0	-	0	-
14	1	Normal (Rare)	1	Normal

15	15	Abnormal (Many)	6	Normal
16	28	Abnormal (Many)	25	Abnormal
17	18	Abnormal (Many)	16	Abnormal
18	20	Abnormal (Many)	20	Abnormal
19	20	Abnormal (Many)	18	Abnormal
20	38	Abnormal (Many)	36	Abnormal
21	15	Abnormal (Many)	16	Abnormal
22	20	Abnormal (Many)	19	Abnormal
23	24	Abnormal (Many)	23	Abnormal
24	0	-	0	-
25	0	-	0	-
26	1	Normal (Rare)	1	Normal
27	0	-	0	-
28	0	-	0	-
29	4	Normal (Rare)	3	Normal
30	0	-	0	-

The resulting R^2 value of 0.976 indicates a high correlation between the system's crystal count output and those obtained from clinical analysis, signifying that the system effectively mirrors clinical measurements. To further evaluate the accuracy of the crystal counting function, three statistical error metrics were calculated. First is the Mean Absolute Error (MAE), which was found to be 0.733 crystals. The value indicates that the average absolute difference between predicted and actual counts was less than one crystal. The formula used for the MAE computation is:

$$MAE = \frac{1}{N}\sum_{i=1}^{N}|y_i - x_i| \quad (3)$$

On the other hand, the Mean Squared Error (MSE) was computed to be 3.533, using the formula:

$$MSE = \sum_{i=1}^{N}\frac{(Predicted_i - Actual_i)^2}{N} \quad (4)$$

Meanwhile, the Root Mean Squared Error (RMSE) was calculated at 1.879, based on the formula:

$$RMSE = \sqrt{\sum_{i=1}^{N}\frac{(Predicted_i - Actual_i)^2}{N}} \quad (5)$$

These results show that most measurements were close to the actual standard values. However, a few outlier cases were identified. For instance, one sample had very small crystals that the system failed to detect. This led to a noticeable increase in the error metrics. Despite this, the overall deviation was still minimal, supporting the reliability of the system for general classification tasks.

4.4. Crystal Classification Accuracy

The YOLOv8 model successfully distinguished calcium oxalate and triple phosphate crystals, achieving a 100% accuracy on the test dataset. Each labeled image was accurately classified, demonstrating the capability of the YOLOv8 model when trained on a well-annotated dataset.

Overall, the system showed excellent performance in detecting and classifying key parameters of urine samples. The pH and turbidity sensors delivered highly accurate readings compared to standard clinical methods. Meanwhile, the imaging and classification system, powered by YOLOv8, successfully counted and identified crystal types with minimal error and high consistency.

4.5. Crystal Classification Accuracy

The YOLOv8 model successfully distinguished between calcium oxalate and triple phosphate crystals, achieving a 100% classification accuracy on the test dataset. Each labeled image was accurately classified, demonstrating the capability of the YOLOv8 model when trained using a well-annotated dataset.

4.6. Performance Metrics

The performance of the system was also assessed by calculating the accuracy, precision, recall, and F1 score values. These metrics can determine how well the system identifies individuals at risk for kidney stones. The confusion matrix is presented below and generated based on the actual validation of the device referenced against the corresponding laboratory results.

Table 3. Confusion matrix

		System Assessment	
Clinical Assessment		Predicted (No Risk)	Predicted (At Risk)
	Actual (No Risk)	21	0
	Actual (At Risk)	1	8

The computed performance metrics reflect how closely the system's assessments align with standard clinical findings. The system achieved an overall accuracy of 96.67%, indicating that it can provide correct assessments in most cases. Only one case, identified as patient number 15, was misclassified. Although this patient had crystals, they were too small for the system to detect, leading to a "No Risk" result despite clinical findings indicating otherwise. Conversely, the

system achieved a precision of 100%, indicating it did not incorrectly label any individual as "At Risk." This is attributed to the logical operation implemented in the system, which only triggers when all measured parameters exceed critical thresholds, preventing false alarms. The recall, on the other hand, was calculated at 88.89%, showing that most patients who were truly at risk were correctly identified by the system. The one misclassification spells out a limitation in detecting very small crystals through imaging. Furthermore, the F1 score was computed at 94.12%. This reflects a strong balance between identifying true positives and minimizing incorrect classifications. These results confirm that the system can offer reliable and timely kidney stone risk assessments in alignment with laboratory standards. Finally, the training and validation results of the object detection model used in the crystal assessment device are also presented in the figure below.

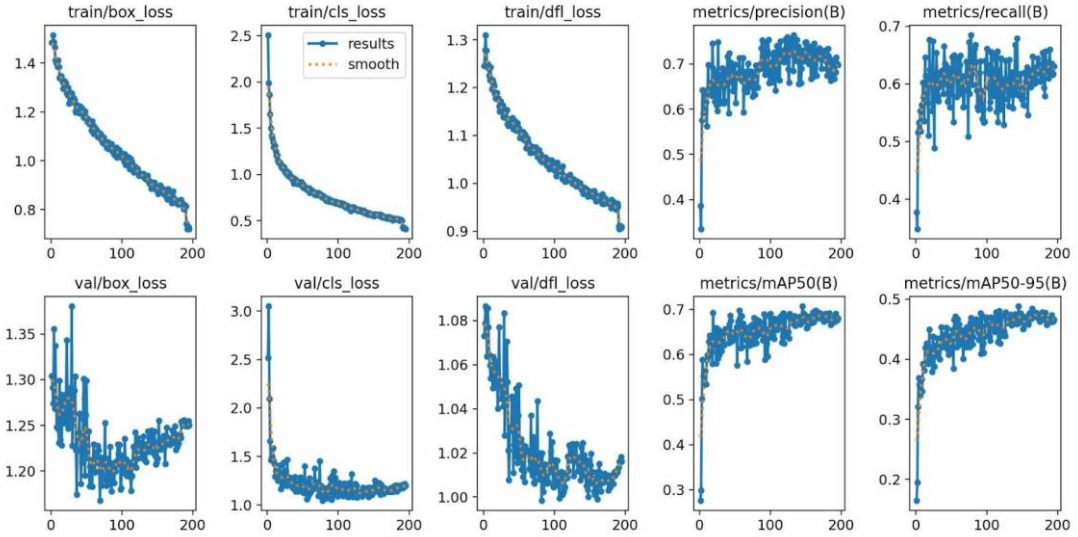

Fig. 14 Object detection model training and validation

During model training and validation, both datasets' loss values consistently decreased. The trend indicates that the model effectively learned from the training samples and generalized well to unseen data. Along with this, improvements in precision, recall, and mean average precision metrics confirmed that the model's performance became increasingly accurate and stable over time. Moreover, the actual testing of the camera and detection model further validated the success of the training process and the model's suitability for practical deployment.

5. Conclusion

The study was centered around developing a compact and integrated system for early detection of kidney stone risk by combining biochemical sensing and image analysis. Using pH and turbidity sensors, along with a YOLOv8 object detection model, the system captured both chemical and visual information from urine samples. Validation was performed with 30 clinical samples, which demonstrated strong alignment with standard laboratory results. Calculated results include an R-squared value of 0.983 for pH detection and 96.67% turbidity classification accuracy. Moreover, an R-squared value of 0.976 was computed with a mean absolute error of 0.733 for crystal counting and 100% accuracy in crystal classification. These results outline the system's reliability in detecting and classifying common urinary crystals such as calcium oxalate and triple phosphate.

The system offers improvements over previously reported techniques by integrating two diagnostic modalities, chemical sensing and microscopic imaging. Prior sensor-based systems lacked the capability to visually confirm the presence or type of urinary crystals, while image-based systems did not consider the chemical conditions promoting crystallization.

This hybrid approach strengthens diagnostic accuracy by allowing each method to complement the limitations of the other, with the logical AND operation serving as the fusion mechanism to deliver conclusive assessments. While the system achieved excellent performance in terms of accuracy and integration, the study recognizes that the computation of inference time or processing latency has not yet been determined. Such measurements are essential for fully validating the system's real-time capability and responsiveness in clinical workflows. Future implementations should include timing analysis to support real-time functionality claims and assess system behavior under more intensive or scaled use cases. Further research is encouraged to expand the types of crystals detectable by the system, integrate additional biomarkers such as protein or specific gravity, and enhance usability features such as wireless connectivity and interface improvements. Multi-centre clinical validation across diverse populations and settings is also recommended to strengthen generalizability and assess effectiveness in rural or resource-constrained environments.

Conflicts of Interest

The authors declare that there is no conflict of interest regarding the publication of this paper. No financial, personal, or professional relationships influenced this research's conduct, analysis, or reporting.

Acknowledgments

Deepest gratitude is extended to the leadership of the College of Engineering for cultivating an environment that supported the researchers' growth and provided valuable resources throughout the project. Sincere appreciation is also expressed to the medical institution that generously accommodated testing requests and provided essential support and data, enriching the study's practical dimension. Equal thanks are given to the panellists whose thoughtful feedback and expertise greatly enhanced the quality of the work. Most importantly, heartfelt appreciation is conveyed to the families and all who offered unwavering support and encouragement, serving as a steady source of strength throughout this academic endeavour. To God be the glory.

References

[1] Firoz Khan et al., "A Comprehensive Review on Kidney Stones, its Diagnosis and Treatment with Allopathic and Ayurvedic Medicines," *Urology & Nephrology Open Access Journal*, vol. 7, no. 4, pp. 69-74, 2019. [CrossRef] [Google Scholar] [Publisher Link]

[2] Mohammed M. A. Abdullah Al-Abdaly et al., "The Influence of Kidney Stones and Salivary Uric Acid on Dental Calculus Formation and Periodontal Status among Some Saudi Patients Aged 25 - 70 Years," *International Journal of Clinical Medicine*, vol. 11, no. 10, pp. 565-578, 2020. [CrossRef] [Google Scholar] [Publisher Link]

[3] Khamidov Obid Abdurakhmanovich et al., "Ultrasound Diagnosis of Urolithiasis," *Central Asian Journal of Medical and Natural Science*, vol. 2, no. 2, pp. 18-24, 2021. [Google Scholar] [Publisher Link]

[4] Kathryn Gillams et al., "Gender Differences in Kidney Stone Disease (KSD): Findings from a Systematic Review," *Current Urology Reports*, vol. 22, no. 10, 2021. [CrossRef] [Google Scholar] [Publisher Link]

[5] John D. Denstedt, "Medical and Surgical Management of Urolithiasis," *Asian Journal of Urology*, vol. 5, no. 4. pp. 203-204, 2018. [CrossRef] [Google Scholar] [Publisher Link]

[6] Leonardo Ferreira Fontenelle, and Thiago Dias Sarti, "Kidney Stones: Treatment and Prevention," *American Family Physician*, vol. 99, no. 8, pp. 490-496, 2019. [Google Scholar] [Publisher Link]

[7] Yu Liu et al., "Epidemiology of Urolithiasis in Asia," *Asian Journal of Urology*, vol. 5, no. 4, pp. 205-214, 2018. [CrossRef] [Google Scholar] [Publisher Link]

[8] Grzegorz Wróbel, and Tadeusz Kuder, "The Role of Selected Environmental Factors and the Type of Work Performed on the Development of Urolithiasis - A Review Paper," *Intnational Journal of Occupational Medicine and Environmental Health*, vol. 32, no. 6, pp. 761-775, 2019. [CrossRef] [Google Scholar] [Publisher Link]

[9] Christine Cudis, Davao City Ranks 3rd in PH with Most Kidney Diseases, Philippine News Agency, 2022. [Online]. Available: https://www.pna.gov.ph/articles/1177310.

[10] Kyriaki Stamatelou, and David S. Goldfarb, "Epidemiology of Kidney Stones," *Healthcare*, vol. 11, no. 3, pp. 1-25, 2023. [CrossRef] [Google Scholar] [Publisher Link]

[11] Nasrin Borumandnia et al., "Longitudinal Trend of Urolithiasis Incidence Rates among World Countries during Past Decades," *BMC Urology*, vol. 23, no. 1, 2023. [CrossRef] [Google Scholar] [Publisher Link]

[12] Zahid Ullah, and Mona Jamjoom, "Early Detection and Diagnosis of Chronic Kidney Disease Based on Selected Predominant Features," *Journal of Healthcare Engineering*, vol. 2023, 2023. [CrossRef] [Google Scholar] [Publisher Link]

[13] Diagnosis of Kidney Stones, National Institute of Diabetes and Digestive and Kidney Diseases (NIDDK), 2017. [Online]. Available: https://www.niddk.nih.gov/health-information/urologic-diseases/kidney-stones/diagnosis.

[14] Flora Rodger, Giles Roditi, and Omar M. Aboumarzouk, "Diagnostic Accuracy of Low and Ultra-Low Dose CT for Identification of Urinary Tract Stones: A Systematic Review," *Urologia Internationalis*, vol. 100, no. 4, pp. 375-385, 2018. [CrossRef] [Google Scholar] [Publisher Link]

[15] Firoz Khan et al., "A Comprehensive Review on Kidney Stones, its Diagnosis and Treatment with Allopathic and Ayurvedic Medicines," *Urology & Nephrology Open Access Journal*, vol. 7, no. 4, pp. 69-74, 2019. [CrossRef] [Google Scholar] [Publisher Link]

[16] Kidney Stone Testing, Tesing, 2021. [Online]. Available: https://www.testing.com/kidney-stone-testing/#:~:text=Blood%20tests%20can%20also%20measure,and%20the%20uric%20acid%20test

[17] Joshua Y.C. Yang et al., "Non-Radiological Assessment of Kidney Stones Using the Kidney Injury Test (KIT), A Spot Urine Assay," *BJU International*, vol. 125, no. 5, pp. 732-738, 2020. [CrossRef] [Google Scholar] [Publisher Link]

[18] Nathaniel P. Roberson et al., "Comparison of Ultrasound versus Computed Tomography for the Detection of Kidney Stones in the Pediatric Population: A Clinical Effectiveness Study", *Pediatric Radiology*, vol. 48, pp. 962-972, 2018. [CrossRef] [Google Scholar] [Publisher Link]

[19] Mohankumar Vijayakumar et al., "Review of Techniques for Ultrasonic Determination of Kidney Stone Size," *Research and Reports in Urology*, vol. 10, pp. 57-61, 2018. [CrossRef] [Google Scholar] [Publisher Link]

[20] Brindha Devi V. et al., "Self-Attention based Progressive Generative Adversarial Network Optimized with Arithmetic Optimization Algorithm for Kidney Stone Detection," *Concurrency and Computation Practice and Experience*, vol. 35, no. 6, 2023. [CrossRef] [Google Scholar] [Publisher Link]

[21] David S.H. Bell, and Edison Goncalves, "Alkalinization of the Urine and Lowering of Urine Uric Acid Content in Diabetic Patients with a Low Urine PH Results in Prevention and Dissolution of Uric Acid Stones - A Case Report and A Retrospective Outcome Study," *Frontiers in Medical Case Reports*, vol. 2, no. 5, pp. 1-4, 2021. [CrossRef] [Google Scholar] [Publisher Link]

[22] C.L. Chang et al., "Primary Hyperoxaluria: The Baragwanath Experience," *South African Journal of Child Health*, vol. 16, no. 2, pp. 89-92, 2022. [CrossRef] [Google Scholar] [Publisher Link]

[23] Tomas Salek et al., "Post-Collection Acidification of Spot Urine Sample is Not Needed before Measurement of Electrolytes," *Biochemia Medica*, vol. 32, no. 2, pp. 194-199, 2022. [CrossRef] [Google Scholar] [Publisher Link]

[24] Sevgi Polat, and Perviz Sayan, "In Vitro Study on the Influence of Proline on Struvite Crystals," *Hittite Journal of Science & Engineering*, vol. 7, no. 4, pp. 271-277, 2020. [CrossRef] [Google Scholar] [Publisher Link]

[25] R.P. Reimer et al., "Detection and Size Measurements of Kidney Stones on Virtual Non-Contrast Reconstructions Derived from Dual-Layer Computed Tomography in an Ex Vivo Phantom Setup," *European Radiology*, vol. 33, no. 4, pp. 2995-3003, 2023. [CrossRef] [Google Scholar] [Publisher Link]

[26] Sevgi Polat, "Effect of Avocado (Persea Gratissima) Leaf Extract on Calcium Oxalate Crystallization," *Acta Pharmaceutica Sciencia*, vol. 58, no. 1, pp. 35-48, 2020. [CrossRef] [Google Scholar] [Publisher Link]

[27] Mohammed I. Rasool et al., "Therapeutic Potential of Medicinal Plants for the Management of Renal Stones: A Review," *Baghdad Journal of Biochemistry and Applied Biological Sciences*, vol. 3, no. 2, pp. 69-98, 2022. [CrossRef] [Google Scholar] [Publisher Link]

[28] Visith Thongboonkerd, "Proteomics of Crystal-Cell Interactions: A Model for Kidney Stone Research," *Cells*, vol. 8, no. 9, pp. 1-12, 2019. [CrossRef] [Google Scholar] [Publisher Link]

[29] Hyperoxaluria, StatPearls Publishing LLC, National Library of Madicine, 2025. [Online]. Available: https://www.ncbi.nlm.nih.gov/books/NBK558987/figure/article-23199.image.f1/

[30] Corey Cavanaugh, and Mark A. Perazellap, "Urine Sediment Examination in the Diagnosis and Management of Kidney Disease: Core Curriculum 2019," *American Journal of Kidney Diseases*, vol. 73, no. 2, pp. 258-272, 2019. [CrossRef] [Google Scholar] [Publisher Link]

[31] Triple Phosphate Crystals, Biron. [Online]. Available: https://www.biron.com/en/glossary/triple-phosphate-crystals/

[32] Wen-Yaw Chung et al., "Development of a Portable Multi-Sensor Urine Test and Data Collection Platform for Risk Assessment of Kidney Stone Formation," *Electronics*, vol. 9, no. 12, pp. 1-18, 2020. [CrossRef] [Google Scholar] [Publisher Link]

[33] Anton Yudhana et al., "Multi Sensor Application-based for Measuring the Quality of Human Urine on First-Void Urine," *Sensing and Bio-Sensing Research*, vol. 34, 2021. [CrossRef] [Google Scholar] [Publisher Link]

[34] Jessie Jaye R. Balbin et al., "Detection and Identification of Triple Phosphate Crystals and Calcium Oxalate Crystals in Human Urine Sediment Using Harr Feature, Adaptive Boosting and Support Vector Machine via Open CV," *ICBET '20: Proceedings of the 2020 10th International Conference on Biomedical Engineering and Technology*, pp. 34-39, 2020. [CrossRef] [Google Scholar] [Publisher Link]

[35] Sania Akhtar, Muhammad Hanif, and Hamidi Malih, "Automatic Urine Sediment Detection and Classification Based on YoloV8," *Computational Science and Its Applications - ICCSA 2023, 23rd International Conference*, Athens, Greece, 2023. [CrossRef] [Google Scholar] [Publisher Link]

[36] Neeraj Dahiya et al., "Optimised RFO Tuned RF-DETR Model for Precision Urine Microscopy for Renal and Systemic Disease Diagnosis," *Scientific Reports*, vol. 15, no. 1, 2025. [CrossRef] [Google Scholar] [Publisher Link]

[37] K.S. Shashikala et al., "Automated Detection of Urine Sediments Using YOLOv8," *2024 3rd International Conference on Automation, Computing and Renewable Systems (ICACRS)*, Pudukkottai, India, pp. 899-904, 2024. [CrossRef] [Google Scholar] [Publisher Link]

[38] Lara Hamawy et al., "Microscopic Urinary Sediments Detection Using Deep Learning," *2024 Second Jordanian International Biomedical Engineering Conference (JIBEC)*, Amman, Jordan, pp. 34-38, 2024. [CrossRef] [Google Scholar] [Publisher Link]

[39] Jie Wang, and Hong Zhao, "Improved Yolov8 Algorithm for Water Surface Object Detection," *Sensors*, vol. 24, no. 15, pp. 1-19, 2024. [CrossRef] [Google Scholar] [Publisher Link]

[40] Nermeen Gamal Rezk et al., "Secure Hybrid Deep Learning for MRI-Based Brain Tumor Detection in Smart Medical IoT Systems," *Diagnostics*, vol. 15, no. 5, pp. 1-17, 2025. [CrossRef] [Google Scholar] [Publisher Link]

[41] Ranjana Battur, and Jagadisha Narayana, "A Novel Approach for Content-based Image Retrieval System using Logical AND and OR Operations," *International Journal of Advanced Computer Science and Applications*, vol. 14, no. 9, pp. 518-528, 2023. [CrossRef] [Google Scholar] [Publisher Link]

[42] Josefine Neuendorf, *Urine Sediment*, Springer Cham, 2020. [CrossRef] [Google Scholar] [Publisher Link]